Journal of Materials Chemistry A

Accepted Manuscript

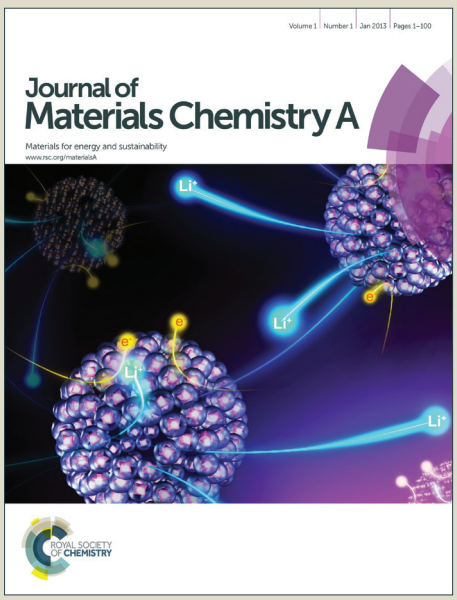

ROYAL SOCIETY OF CHEMISTRY

www.rsc.org/materialsA

In situ X-ray pair distribution function analysis of accelerated carbonation of a synthetic calcium-silicate-hydrate gel

Antoine E. Morandeau[a], Claire E. White[a*]
[a] Department of Civil and Environmental Engineering and the Andlinger Center for Energy and the Environment, Princeton University, Princeton NJ, USA

Keywords: Amorphous material; Calcium–silicate–hydrate (C–S–H); Carbonation; Reaction kinetics; X-ray diffraction;

Electronic supplementary information (ESI) available: Detailed description of synthesis and characterisation of the calcium-silicate-hydrate gel: Rietveld and real space refinement details and results. See DOI: xxx

Abstract
Calcium-silicate-hydrate (C-S-H) gel is the main binder component in hydrated ordinary Portland cement (OPC) paste, and is known to play a crucial role in the carbonation of cementitious materials, especially for more sustainable alternatives containing supplementary cementitious materials. However, the exact atomic structural changes that occur during carbonation of C-S-H gel remain unknown. Here, we investigate the local atomic structural changes that occur during carbonation of a synthetic calcium-silicate-hydrate (C-S-H) gel exposed to pure CO_2 vapour, using in situ X-ray total scattering measurements and subsequent pair distribution function (PDF) analysis. By analysing both the reciprocal and real-space scattering data as the C-S-H carbonation reaction progresses, all phases present during the reaction (crystalline and non-crystalline) have been identified and quantified, with the results revealing the emergence of several polymorphs of crystalline calcium carbonate (vaterite and calcite) in addition to the decalcified C-S-H gel. Furthermore, the results point toward residual calcium being present in the amorphous decalcified gel, potentially in the form of an amorphous calcium carbonate phase. As a result of the quantification process, the reaction kinetics for the evolution of the individual phases have been obtained, revealing new information on the rate of growth/dissolution for each phase associated

with C-S-H gel carbonation. Moreover, the investigation reveals that the use of real space diffraction data in the form of PDFs enables more accurate determination of the phases that develop during complex reaction processes such as C-S-H gel carbonation in comparison to the conventional reciprocal space Rietveld analysis approach.

1.Introduction

Calcium-silicate-hydrate (C-S-H) gel is an important nanocrystalline and heterogeneous phase that exists in hydrated ordinary Portland cement (OPC) paste. This phase is known to control important performance and durability aspects of OPC-based concrete, including permeability and shrinkage,[1] and is also affected by chemical degradation mechanisms such as carbonation.[2] Therefore, it is crucial that this phase is well-characterised across a range of length scales, including having a full understanding of the atomic structural changes that occur when exposed to different degradation environments. The atomic structure and associated properties of C-S-H gel have been investigated in the past using a variety of experimental and theoretical techniques.[2–9] However, due to the non-crystalline and heterogeneous nature of this material, the atomic and nanoscale structure is still being debated in the literature.[10,11] Nevertheless, recently new information has been obtained using the total scattering method,[4,5,9] which utilises X-ray and/or neutron scattering data and the associated pair distribution function (PDF) to obtain real-space information on the atom-atom correlations present in the material. A PDF investigation on one type of C-S-H gel (synthetically synthesised) has revealed that the atomic structure with a Ca/Si ratio of 1 ± 0.15 consists of local and medium range ordering similar to 11 Å tobermorite.[4]

Carbonation of C-S-H gel is an important chemical degradation process controlling concrete durability. Carbonation of C-S-H gel will occur naturally under atmospheric conditions, and consists of the removal of calcium ions from the gel leading to the formation of an amorphous silica

gel and various polymorphs of calcium carbonate: amorphous calcium carbonates (ACC), calcite, vaterite and/or aragonite. The transformation of C-S-H gel to an amorphous silica gel due to carbonation is described in Eq. (1).

$$(CaO)_x(SiO_2)(H_2O)_z + x\,CO_2 \rightarrow x\,CaCO_3 + SiO_2(H_2O)t + (z-t)H_2O \quad (1)$$

Several investigations have been conducted on the atomic structure of C-S-H gel and the changes that occur as a result of carbonation using a range of experimental techniques including Raman spectroscopy[12,13] and X-ray photoelectron spectroscopy (XPS).[2] The Raman spectroscopy investigation on carbonated C-S-H gel revealed that the extent of decalcification is strongly linked with the initial Ca/Si ratio of the gel.[13] Gels with high Ca/Si ratios (Ca/Si ~ 1.5) were seen to contain a large number of dimeric silicate anions (Q^1 sites) prior to carbonation,[12] which were more susceptible to reorganisation as a result of carbonation compared silicate chain units (Q^2 sites). This reorganisation process of the gel consists of the polymerisation of the silicate species to form the silica gel (Q^4 sites).[2] Furthermore, these authors observed the presence of ACC in the carbonated gels during the initial stages of the carbonation reaction, that later transformed into crystalline calcium carbonate polymorphs vaterite and aragonite.[13] Aragonite was present only when Raman bands attributed to Q^4 silicates were observed, and therefore the investigation concluded that aragonite precipitation is favoured in the presence of amorphous silica.[13]

The kinetics of C-S-H gel carbonation and associated evolution of the individual phases (crystalline calcium carbonate polymorphs and decalcification of C-S-H gel) has been investigated by Castellote et al.,[14] where carbonation of plain cement paste exposed to 100% CO_2 was monitored using in situ neutron diffraction. The results revealed an exponential decay of the CH, C-S-H gel and ettringite content over time.[14] However, the investigation concentrated on the kinetics of the

carbonation reaction, as opposed to a detailed study of the structural changes occurring to the C-S-H gel, and therefore the exact atomic structural changes that occurred during carbonation of C-S-H gel were not analysed or reported. Hence, although the C-S-H gel carbonation reaction has been investigated in the past, revealing important information on the local bonding environments (Raman spectroscopy and XPS) and crystalline phases (diffraction), the local and medium range atomic structural information have not been analysed, which contains details such as the reorganisation of the silica polyhedra in the decalcifying gel and ordering present in the amorphous silica gel.

In this work, the local and medium range ordering of a synthetic C-S-H gel have been measured using X-ray PDF analysis together with the changes induced due to carbonation. By performing both reciprocal and real-space fitting of the data, the kinetics of reaction for various phases that evolve has been obtained and analysed. Furthermore, the local structural nature of the amorphous silica gel that forms as a result of C-S-H gel carbonation has been assessed, especially in terms of further structural evolution that occurs as the reaction proceeds.

2.Materials and methods

2.1 C-S-H synthesis and characterisation

C-S-H gel was synthesised using a double decomposition method with calcium nitrate and sodium silicate as the starting materials.[15] During each step of the synthesis, precautions were taken to avoid early carbonation by working under a flow of industrial-grade nitrogen. Each solution was prepared with chemicals from Sigma-Aldrich and deionised water. 6.10 g of reagent-grade Na_2SiO_3 powder was dissolved in 125 ml of water (to obtain a 0.050 molar solution), and then stirred for 24 hours in order to ensure full dissolution of Na_2SiO_3. A separate solution of 0.075 molar of reagent-grade $CaNO_3$ was synthesised by dissolving 13.06 g of $CaNO_3 \cdot 4H_2O$ in 75 ml of water. The two

solutions were added together, and then shaken manually for 15 min. The C-S-H precipitate was then filtered using a Buchner funnel and washed with a 2L calcium hydroxide solution with a concentration of a 20 mM. After the wash solution had passed through the solid, the sample was flushed with nitrogen and tightly sealed in a plastic container for one month.

The Ca/Si ratio of the as obtained C-S-H gel was quantified by X-ray Fluorescence Spectroscopy (XRF, Rigaku Supermini). The C-S-H used for the XRF analysis was dried at 105°C until equilibration of the mass, at which point it was mixed with a cellulose binder in order to make a flat pellet. This pellet was analysed in the XRF under vacuum. The results revealed that the Ca/Si ratio of the synthesised C-S-H gel was approximately 1.4 with no traces of Na, Mg or NO_3.

2.2 X-ray data collection and analysis

Detailed information on the methods can be found in the Supplementary Information. For the X-ray PDF measurements the C-S-H gel was loaded into a 1 mm diameter polyimide capillary which was then sealed using porous glass wool in order to enable the gases (Ar and CO_2) to flow through the sample. The capillary was then mounted and aligned in the gas cell[16] on the 11-ID-B beamline at the Advanced Photon Source, Argonne National Laboratory, under ambient temperature conditions. The sample was analysed using a wavelength of 0.2114 Å and a two-dimensional image plate detector.[17] The detector was located 167 mm from the sample. Data collection commenced under a flow of Ar for the first 2 min to obtain data on the initial (non-carbonated) C-S-H gel. Then the gas was switched to CO_2 (100%), and data sets were acquired every 30 s for a duration of 4 minutes, after which the scan times were extended to every 2 min. These measurements continue for ~ 3hrs, after which no significant changes in the local structure were detected. The data conversion from 2D to 1D was carried out using the program Fit2D with CeO_2 as the calibration material.[18,19]

Reciprocal space analysis has been carried out using the Rietveld method[20] and the Maud software.[21] Details of the refinement process are given in the Supplementary Information. The scale factors of C-S-H gel (ICSD #187041[22]), calcite (ICSD #18166[23]) and vaterite (COD #913565[24,25]) were refined in order to quantify the evolution of these phases as an extent of the carbonation reaction, and therefore to obtain information on the kinetics of reaction with respect to a particular phase (i.e., C-S-H gel, calcite and vaterite).

The real space analysis was carried using the PDF data. This function (G(r)) is obtained by taking a sine Fourier transform of the measured total scattering function, S(Q), as shown in Eq. (2) , where Q is the momentum transfer given in Eq. (3).[26]

$$G(r) = \frac{2}{\pi}\int_{Q_{min}}^{Q_{max}} Q[S(Q) - 1]\sin(Qr)dQ \quad (2)$$

$$Q = \frac{4\pi\sin\theta}{\lambda} \quad (3)$$

Standard data reduction procedures were followed to obtain the PDF using PDFgetX2,[27] with a Q_{max} of 20 Å^{-1}. The instrument parameters were elucidated by measuring a nickel standard (Sigma-Aldrich) and performing a refinement using the PDFgui software.[28] The refined parameters were Q_{broad} = 0.0196 Å^{-1} and Q_{damp} = 0.0347 Å^{-1}.

To quantify the extent of reaction in real space, a methodology was used similar to that outlined in a previous article[29] where the initial and final PDF data sets from an in situ diffraction experiment were used as the start and end points for quantification. The intermediate data sets were then fitted

over various *r* ranges (in Å) using a linear combination of the initial and final data sets (Eq. (4)), where α is between 0 and 1).

$$G(r)_{calc} = (1-\alpha)initial + \alpha final \quad (4)$$

In this investigation, the best fit has been obtained by minimising $\Sigma[(G(r)_{calc} - G(r)_{exp})^2]$ with respect to α for each intermediate data set ($G(r)_{exp}$), giving the α value (or extent of carbonation reaction), where α = 0 corresponds to the initial data set, and α = 1 corresponds to the final data set (fully reacted). The linear combination method was carried out using Matlab, where α was varied in increments of 0.001, and the value of α that gave the best fit (smallest difference) being the value reported in the Results and Discussion section.

The PDF of the amorphous silica gel $G(r)_{am}$ existing in the fully-carbonated sample was obtained by subtracting out the contributions from the crystalline phases, calcite and vaterite, with the remaining atom-atom correlations being attributed to the decalcified amorphous silica gel. This subtraction procedure was achieved by simulating the PDFs of calcite ($G(r)_{calcite}$) and vaterite ($G(r)_{vaterite}$) using PDFgui,[28] which were subsequently subtracted from the experimental data set. The atomic structures for calcite and vaterite were refined (lattice parameters (*a*, *b* and *c*), atomic displacement parameters (u_i) and scale factors) over the range $40 < r < 65$ Å for the fully carbonated PDF data set (3 hrs) since previous investigations have revealed that C-S-H gel contributes to atom-atom correlations only below ~ 40 Å.[4,9] The calcium carbonate structures chosen were calcite[23] (ICSD #18166) and vaterite[24,25] (COD #913565). It should be noted that the structure of vaterite is still being debated in the literature[24,25,30], and therefore careful choice of a representative structure was necessary. Due to the need to avoid vaterite structural representations containing partial site occupancies, which would artificially create infeasible atom-atom correlations at low *r* values, the structure proposed by Wang et al.[24,25] based on density functional theory calculations was selected.

Detailed procedures for the refinement are given in the Supplementary Information.

3.Results and discussion

3.1 Reciprocal space analysis

The X-ray diffraction patterns of (i) C-S-H gel and (ii) the changes occurring to the C-S-H gel during carbonation are displayed in Fig. 1, where the scattered intensity, I(Q), has been normalised by the incoming photon flux. It is clear in Fig. 1 that the nanocrystalline phase C-S-H gel is initially present in the sample prior to carbonation, and as the carbonation reaction proceeds, the crystalline phases, calcite and vaterite, increase in intensity. Apart from the C-S-H gel phase, a relatively small amount of calcite (~ 7 wt. % calculated using Rietveld analysis) is also present prior to carbonation, which implies that the sample did carbonate slightly before to the beginning of the measurement. The presence of vaterite in Fig. 1 is visible via the Bragg peaks located at Q values of 1.76, 1.90 and 2.30 $Å^{-1}$,[24,25] while calcite is identified by the peaks located at Q values of 2.51 and 2.74 $Å^{-1}$. [23] The main peak at a Q value of 2.06 $Å^{-1}$ is attributed both to C-S-H gel[22] and calcite, and is seen to decrease in intensity as the carbonation reaction proceeds. Due to the increase in Bragg peaks associated solely with calcite as the reaction progresses, the decrease in the C-S-H gel/calcite peak is associated with the decalcification of the gel.

Fig. 2 displays the results of the Rietveld refinement as a function of carbonation time, where the mass fractions for the various (nano)crystalline phases are reported as the reaction progresses. The time necessary for the CO_2 to travel from the gas valve-switch to the sample (2.4 min) has been subtracted from the data. It is clear from Fig. 2 that a rapid formation of vaterite and calcite occurs as soon as the CO_2 vapour reaches the capillary. This behaviour is accompanied by the fast reduction in intensity of the C-S-H gel, which is attributed to C-S-H gel decalcification. During the

initial 20 to 30 minutes of reaction the rate of decalcification of C-S-H gel and the formation of vaterite are both linear in nature, whereas the formation of calcite follows an exponential decay trend (given in Eq. (5)). In terms of thermodynamic stability, vaterite is the least stable phase among the three anhydrous crystalline calcium carbonate polymorphs: calcite, aragonite, and vaterite.[31] However, previous investigations have revealed that all three crystalline phases together with ACC[32] have been observed in naturally carbonated OPC paste[33] and for pastes subjected to accelerated conditions.[33,34] Specifically, a high CO_2 concentration leads to the formation of the less thermodynamically stable phases (vaterite or aragonite),[35,36] while the relative humidity (RH) controls the formation of ACC together with the crystalline polymorphs, with a low RH (< 20%) favouring the formation of ACC, intermediate RH (20 < RH < 60%) leading to the coexistence of all three crystalline phases, and high RH favouring only the formation of calcite.[32] The Ca/Si ratio of the C-S-H gel is also seen to influence the formation of various calcium carbonate polymorphs during carbonation, with lower Ca/Si ratios (approx. < 1.0) favouring the formation of vaterite and aragonite over calcite.[13]

$$\frac{m_{calcite}(t)}{m_{total}} = A \times \left(1 - \exp^{\frac{-t}{\tau_{calcite}}}\right) + B \quad (5)$$

After the initial stage of carbonation has finished (after ~27 min), subsequent exposure to CO_2 appears to result in a slow transformation of vaterite to the more stable form of calcite. A previous investigation on this transformation from vaterite to calcite using the solution-based synthesis method revealed that this transformation is strongly dependent on the temperature, and for ambient conditions takes approx. 6 hrs or more, with the majority of changes seen to occur in the last 3 hrs.[37] Hence, further changes are expected to occur beyond the time scale depicted in Fig. 2, with the dominant process being the slow transformation of vaterite to calcite. Later in this investigation the

PDF data will be analysed to assess if the same behaviour (slow transformation of vaterite to calcite) is obtained from the real space information.

The rate of formation of calcite does not abruptly change once the calcium in C-S-H gel has been depleted, and instead calcite then continues to form at the expense of vaterite, it is clear that the kinetics controlling calcite formation are independent of the rate of C-S-H gel decalcification (above a certain CO_2 partial pressure). This is probably due to the fact that the pore solution is supersaturated with respect to carbonate phases (due to 100% CO_2 gas flow and rapid decalcification of C-S-H gel) and thus the maximum calcite growth rate is reached and is the limiting kinetic factor. Since the solubility product of vaterite is greater than calcite (K_{sp} $10^{-7.913}$ compared to $10^{-8.480}$ for calcite[31]), the data appear to suggest that the solution remains supersaturated by the preferential dissolution (buffering) of vaterite once all of the calcium has been leached from the C-S-H gel.

Fitting the first order rate expression (Eq. (5)) to the calcite data in Fig. 2 results in an initial content (B in fractional amount, where 1.0 equates to all calcite) of 0.074, while amplitude at the completion of reaction (A + B) is 0.451 ± 0.004 and the characteristic time of reaction ($\tau_{calcite}$) is 23.6 ± 0.7 min. C-S-H gel carbonation has been analysed in the past using neutron diffraction and the Rietveld method. Castellote et al.[14] investigated carbonation of OPC paste using neutron diffraction and 100% CO_2 as the gas supply. However, in their study the C-S-H gel content was not easily quantified due to limited instrument resolution combined with the presence of portlandite in the sample. Vaterite formation was not observed, which may also be due to the limited resolution data and/or portlandite carbonation dominating the diffraction pattern. Furthermore, Castellote et al. controlled the relative humidity (at 65%) by using a saturated saline solution,[14] whereas in our case the relative humidity was not controlled and most likely was lower which explain the presence of

vaterite in higher quantity compared to calcite.[32] It is important to note that calcite molar volume is 36.8 $cm^3.mol^{-1}$, compared to 39.0 $cm^3.mol^{-1}$ for vaterite (calculated from the Rietveld refinement results). Hence, for certain accelerated testing conditions, where the CO_2 concentration is relatively high, this difference in molar volume together with the presence of vaterite in addition to calcite will affect/change the porosity, and thus the transport properties in the porous media when compared to natural conditions. Furthermore, the transport properties will also be affected by the fact that these crystals can grow in the C-S-H gel pores or on the surface of the agglomerated gel particles. This could be answered by a microstructural study investigating the discrepancy between thermodynamic and kinetic effects concerning the precipitation/dissolution of the various crystalline calcium carbonate polymorphs, specifically to assess the nucleation location of vaterite and calcite.

3.2 Real space analysis: C-S-H gel carbonation

The X-ray PDFs of the carbonation reaction of C-S-H gel are displayed in Fig. 3. The initial (non-carbonated) C-S-H gel PDF has been compared to the experimental results obtained by White et al.[9] for synthetic C-S-D gels (where D stands for deuterated water) in the Supplementary Information, with the results showing that the double decomposition method is successful in replicating the local atomic structure and nanocrystalline nature of this important OPC phase. As the carbonation reaction proceeds in C-S-H gel (Fig. 3), there are evident changes in all atom-atom correlations related to the crystalline calcium carbonate polymorphs, specifically the C-O, Ca-C and Ca-O correlations, which increase in intensity. On the other hand, the main correlation pertaining to the C-S-H gel, namely Ca-Si, drastically diminishes in intensity. In the dreierkette-based models for C-S-H gel,[3] the silica chain paired to the central Ca-O layer gives rise to the Ca-Si correlation seen in Fig. 3, and therefore as C-S-H gel is exposed to CO_2, the removal of calcium atoms (decalcification) from the layered chain structure leads to a reduction in the number of Ca-Si correlations in the material. The medium range order is also affected by the carbonation reaction, as

seen by the changes in intensity in Fig. 3 due to the (i) decalcification of C-S-H gel, and (ii) precipitation of calcite and vaterite. The change in kinetics once all calcium has been removed from the C-S-H gel is particularly noticeable in Fig. 3, which coincides with the arrestment of vaterite formation (occurs at ~27 min). This behaviour is evident in the C-O correlation at 1.26 Å, where the correlation stops increasing in intensity at some stage between 20 and 30 min. Furthermore, the correlation at 6.5 Å is seen to stop changing between 20 and 40 minutes, only to increase in intensity at a different *r* value towards the final stages of the reaction. Other atom-atom correlations in this region are seen to follow smooth transitions over the entire reaction time, and therefore are either (i) indicative of C-S-H gel changes, or (ii) correlations that are common to both calcite and vaterite.

In order to assess the rate of change for specific atom-atom correlations present in Fig. 3 together with the overall reaction kinetics from the X-ray PDF data, the data have been analysed using the quantification method outlined in the Supplementary Information for different *r* ranges, with the results given in Fig. 4 (extent of reaction (α) as a function of time). Interestingly, not all of the fitting ranges give the same profile for the extent of reaction, as is evident by the Si-O and Ca-O correlations in Fig. 4, where they possess slower kinetics compared to the other regions (e.g., C-O). For the Si-O correlation, this behaviour is indicating that there are subtle changes occurring to the local environment of the silicon atoms as the C-S-H gel transitions to the amorphous silica gel. Furthermore, since the Si-O extent of reaction in Fig. 4 does not reach the same plateau as the majority of the other profiles, it is likely that the silica gel is undergoing structural reorganisation during the later stages of reaction, even after the majority of the calcium has been removed from the gel. Likewise, the delay in the Ca-O correlation peak in Fig. 4 indicates that the local environment of the calcium atoms is different in C-S-H gel and vaterite/calcite, and therefore, the slower transformations during the later stages of reaction (such as from vaterite to calcite, or the

continuation of leaching of calcium from the C-S-H gel) are accompanied by changes in the Ca-O atom-atom correlation.

3.3 Atomic structure of amorphous silica gel

The PDF of the amorphous silica gel after removal of the crystalline components from the fully-carbonated data set (C-S-H gel exposed to CO_2 for 3 hrs), is given in Fig. 5. Also provided in this figure is the original data set for the fully-carbonated sample together with the fit obtained by refining the calcite and vaterite content. This figure includes an insert showing correlations present above 7 Å, where good agreement between the experimental PDF of the carbonated C-S-H gel and the refined contributions from calcite and vaterite is obtained. The residual product of C-S-H gel carbonation shown in Fig. 5 reveals that this silica gel possesses mostly short range order (as opposed to containing strong atom-atom correlation beyond ~ 10 Å) and therefore is predominately amorphous.

The local atomic structure of silica gel (Fig. 5) consists of a dominant Si-O correlation at 1.63 Å, along with a smaller remnant Ca-O peak which indicates that some remaining calcium is trapped within the gel, or is not accessible to form carbonation products. This may be due to kinetic effects since this data was obtained 3 hours after the commencement of the accelerated carbonation experiment, and therefore the residual calcium in the silica gel may be accessible for reaction at longer time scales. However, this result where calcium is still present in the sample corroborates previous carbonation investigations (10% CO_2 accelerated conditions) on cement paste which revealed that not all the calcium present in the C-S-H gel is available for carbonation.[33,38,39] C-S-H gels with higher density[39] or lower initial Ca/Si ratios are harder to fully decalcify.[2] However, it remains unknown if this residual calcium is trapped as (i) a separated phase such as ACC, or (ii) is distributed homogeneously throughout the silica gel. Furthermore, the observance of the Ca-O peak

in silica gel in Fig. 5 warrants further investigation, especially since the atomic structure of vaterite is still an area of open debate, and therefore the simulated Ca-O shown in Fig. 5 for calcite/vaterite may not be accurate, with the low *r* shoulder of this simulated peak possibly accounting for the significant differences seen at maximum peak intensity. A future PDF investigation of vaterite would be able to rectify these uncertainties.

3.4 Evolution of the amorphous/nanocrystalline phase during carbonation

The crystalline contributions present in the PDFs have been removed by refining the scale factors for both crystalline polymorph as a function of time (as outlined in the Supplementary Information). The evolution of the scale factors for calcite and vaterite as the reaction progressed are shown in Fig. 6, together with the goodness of the fit (R_w, as defined in PDFgui[28]). This figure reveals that the formation of calcite and vaterite, as obtained from the real space PDF data, follows a similar trend to the reciprocal space Rietveld results (Fig. 2), especially for the case of vaterite, which is seen to increase linearly during the initial stages of reaction, and then plateaus after ~ 27 minutes. On the other hand, the evolution of calcite does not closely follow a first order rate expression, and initially a much greater percentage of calcite is present (15% by mass) compared to the Rietveld result. It is important to note that the absolute values for scale factors is semi-quantitative without the use of an internal standard, and therefore the percentage of calcite initially present prior to accelerated carbonation is a rough estimate. Nevertheless, the real space data reveals that a higher amount of calcite exists in the sample prior to carbonation, and the evolution of the two calcium carbonate polymorphs do not follow the exact same trends as obtained using reciprocal space analysis (Fig. 2).

There are distinct differences between the reciprocal and real space data for the evolution of the

crystalline phases during the carbonation reaction. For the reciprocal space data it was necessary to (i) fit a background function and (ii) simulate the atomic structure of the initial C-S-H gel. Furthermore, any resulting amorphous silica gel was not explicitly simulated, and instead was encapsulated in the increasingly dominant background function. On the other hand, for the real space PDF data there were no assumptions made regarding the structure of the C-S-H gel and resulting amorphous silica gel, since only the high *r* data was fitting, beyond the distances where these amorphous/nanocrystalline phases contribute. Furthermore, due to the careful subtraction process required in order to produce the X-ray PDFs, no assumptions/fitting was needed for the background since this was measured and subtracted prior to performing the sine Fourier transform.

The evolution profile of the vaterite scale factor during the C-S-H carbonation reaction is dependent on the form of the diffraction data (reciprocal and real space data, Fig. 2 and Fig. 6, respectively). From the Rietveld refinement, vaterite is seen to increase in mass fraction beyond the final value reached at 3 hrs, and therefore dissolves slightly during the later stages of reaction due to the continual increase in mass fraction of calcite. On the other hand, the real space data (Fig. 6) reveals that once the vaterite fraction reaches a maximum there is no further increase or decrease in this value. Although Fig. 6 shows that the calcite fraction continues to grow past ~ 27 min, this growth is not at the expense of vaterite. Instead, another source of calcium must be readily available for calcite growth and is attributed to either the decalcifying C-S-H gel and/or ACC.

The X-ray PDFs of the carbonating C-S-H gel after removal of the contributions from calcite and vaterite are displayed in Fig. 7. The 'initial' PDF is the non-carbonated C-S-H gel without the contributions from calcite. As the carbonation reaction proceeds, the Si-O correlation peaks at 1.63 Å greatly increases as a result of the change (decrease) in atomic number density (ρ_0), which indicates that the atomic structure of the amorphous silica gel is less dense compared to the original

C-S-H gel. As the carbonation reaction progresses the Ca-O peak at 2.38 Å decreases as calcium ions are removed from the C-S-H gel. Also shown in Fig. 7 is the long range ordering ($7 < r < 30$ Å) of the initial (C-S-H gel) and final (amorphous silica gel) PDF curves, where it is apparent that the silica gel contains less ordering at this length scale, and therefore the decalcifying C-S-H gel evolves towards a structure with predominately short range ordering.

It was earlier discussed that in contrast to the Rietveld refinement results, which stated that at later stages of the reaction vaterite provides the calcium ions for further calcite formation, the PDF analysis revealed that another source of calcium was responsible for the later stages of calcite formation since the scale factor for vaterite remains relatively constant at ~ 0.37 after 27 min of reaction. Figs. 3 and 7 reveal that there are small changes still occurring to the Ca-Si correlation at ~ 3.60 Å beyond 30 min, which indicates that calcium ions are still being leached from the partially-decalcified C-S-H gel during the later stages of the reaction. These ions are then reacting with carbonate molecules to form more calcite. The additional peaks that arise during the carbonation reaction at *r* values of ~ 4.20 and 5.17 Å are attributed to formation of the amorphous silica gel, and have been documented in previous investigations.[40,41] However, it is important to note that prior to drawing definitive conclusions regarding the exact atom-atom correlations present in the decalcified C-S-H gel/amorphous silica gel, it is necessary to obtain accurate PDF data on calcite and vaterite. Currently it cannot be ruled out that some of the atom-atom correlations in Fig. 7, especially at low r, arise due to non-ideal structural representations for vaterite and calcite. This is particularly apparent in the correlation present at ~ 3.22 Å in Fig. 7, which increases in intensity as the reaction progresses. Interestingly, this correlation is also seen to be present in ACC,[42,43] and therefore may indicate that ACC exists in the sample. Hence, further analysis is required to determine if this correlation is attributed to non-ideal structural representations of vaterite and calcite, and therefore erroneous subtraction of the crystalline phases at low *r* values (< 5 Å), or if the correlation is real

and potentially due to the emergence of ACC during the carbonation reaction. An overview of the phases present during C-S-H carbonation and the reaction sequence elucidated in this investigation are given in Eqs. (6) and (7), where Eq. (7) Shows the later stage transformation of ACC to the most stable crystalline polymorph (calcite).

$$C-S-H + carbon\ dioxide \rightarrow ACC + Calcite + Vaterite + Silica\ gel \quad (6)$$

$$ACC \rightarrow Calcite \quad (7)$$

3.5 Reciprocal versus real space analysis of cementitious systems

As highlighted in the previous section, the use of real space diffraction data in the form of PDFs enables more accurate determination of the phase evolution during complex reaction processes such as C-S-H gel carbonation in comparison to the conventional reciprocal space Rietveld analysis approach. The advantage of using real space data is attributed to the fact that the crystalline contributions in the sample can be successfully isolated from the amorphous/nanocrystalline contributions without the need for prior knowledge of the exact atomic structure existing in this non-crystalline phase(s). This is achieved by only refining the contributions from the crystalline phases over an *r* range that is beyond the atom-atom distances attributed to the non-crystalline phases (> 40 Å in this investigation). On the other hand, for Rietveld analysis, prior knowledge is needed on the exact structures of the non-crystalline phases to ensure that an accurate quantification of all the phases is obtained. As seen by the differences between Figs. 2 and 6, Rietveld analysis infers that all the C-S-H gel is depleted by ~27 min, at which stage further calcium is obtained via dissolution of vaterite, however, from real space analysis of the data it is seen that calcium remains in the partially-decalcified C-S-H gel at 27 min, and this calcium in addition to possible calcium in ACC, enables further formation of calcite (potentially via formation of vaterite and aragonite).

This discrepancy in results (i.e., nature of vaterite formation/dissolution) between reciprocal and real space analysis is attributed to the nature of the information in reciprocal space, where amorphous, nanocrystalline and crystalline phases contribute to the entire diffraction pattern. Although the amorphous components tend to be noticeable via broad diffraction peaks located in a particular region in the diffraction pattern, information on the real space atom-atom correlations is present as frequencies in reciprocal space, and therefore spans the full range of measured data. On the other hand, the real space PDF data can be segmented in *r* according to the type of phases present in the sample. For the case of C-S-H gel carbonation, this segmentation has been carried out at 40 Å, above which only the crystalline phases are seen to contribute to the data. Hence, this makes it possible to accurately determine the evolution of these crystalline phases without the need to make assumptions regarding the scattering signals from the non-crystalline components. Furthermore, even though appropriate structural models of C-S-H gel are available in the literature that replicate the diffraction data in reciprocal space, there are no such models available as this gel decalcifies, and therefore assumptions have to be made regarding the nature of the gel during decalcification. Real space analysis using the PDF technique is well-poised for circumventing these limitations associated with Rietveld analysis, since our real space PDF subtraction approach only requires the use of structural models for the crystalline phases. This investigation has served as a proof of principle study of the atomic structural changes that occur to the non-crystalline phases during carbonation of C-S-H gel, and it is important to keep in mind that the CO_2 concentration employed during the experiment is high. Future work should include application of this method using more realistic CO_2 concentrations for accelerated testing scenarios. Other potential applications of this form of analysis include the cement hydration reaction (hydration of C_3S), hydration of OPC and chemical degradation processes such as sulphate attack.

4. Conclusion

The results presented in this investigation have revealed that in situ X-ray PDF analysis is a valuable method for investigating the atomic structural changes that occur during carbonation of C-S-H gel, particularly since this process involves the dissolution and formation of amorphous/nanocrystalline phases that are extremely difficult to fully characterise using the conventional X-ray diffraction approach (Rietveld analysis). Both reciprocal and real space results reveal that during the initial stages of the carbonation reaction a rapid formation of the calcium carbonate crystalline polymorphs occur (vaterite and calcite) during the initial 27 min of reaction, which corresponds to the period during which calcium is still readily available in the partially-reacted C-S-H gel. During the later stages of the reaction a slow rate of transformation from vaterite to calcite is observed from Rietveld analysis, however, this result is likely erroneous due to the absence of accurate structural models of the decalcifying C-S-H gel.

More accurate results for the C-S-H gel carbonation reaction are obtained using real space PDF analysis, which reveals that calcium is still available in the partially-decalcified C-S-H gel after 27 min of reaction, and it is this source of calcium that contributes to the continual formation of calcite throughout the reaction. Furthermore, there is the possibility that ACC is present during the carbonation reaction, and may be the source of calcium during the later stages for calcite formation. Analysis of the calcite rate of formation provides important kinetics-based information regarding the dominant reactions controlling this process, where calcite formation is the rate limiting factor and excess calcium and carbonate ions in the supersaturated solution lead to the formation of vaterite (and potentially ACC). Via analysis of the PDF data, including the removal of the crystalline phases, this investigation reveals the exact atomic structural changes that occur as nanocrystalline C-S-H gel transforms to amorphous silica gel. The data directly shows the loss of medium range atom-atom correlations during the decalcification process of the gel together with the

emergence of new correlations at low *r* attributed to the silica gel (and potentially ACC). Hence, this investigation serves as an important step towards elucidating the exact structural changes that occur during a complex reaction processes such as C-S-H gel carbonation, and there is significant potential for similar approaches to be adopted in the research community in order to further characterise other important reaction processes relating to cementitious materials.

Acknowledgments:

This work was financially supported by the Princeton E-ffiliates Partnership award, Andlinger Center for Energy and the Environment (Princeton University). We gratefully acknowledge the assistance and guidance provided by Karena Chapman and Kevin Beyer for their help with the gas cell. The 11-ID-B beam line is located at the Advanced Photon Source, an Office of Science User Facility operated for the U.S. DOE Office of Science by Argonne National Laboratory, under U.S. DOE Contract No. DE-AC02-06CH11357.

List of figures:

Figure 1. X-ray diffraction patterns of C-S-H gel as a function of the carbonation time. The initial diffraction pattern is for C-S-H gel prior to exposure to CO_2 vapour.

Figure 2. Evolution of the (nano)crystalline phases during C-S-H gel carbonation, obtained using Rietveld quantification of X-ray diffraction data. The normalised calcite mass evolution has been fitted using a first order rate equation (exponential function given in Eq. (5)).

Figure 3. Evolution of the X-ray PDF of C-S-H gel as a function of the carbonation time. Peak assignments are given based on references.[41,44]

Figure 4. Extent of the carbonation reaction as a function of time for various fitting ranges of the X-ray PDF data. The full range is defined as 0.01 < r < 50 Å.

Figure 5. X-ray PDF data of C-S-H gel after 3 hours of accelerated carbonation (#1) and simulated contributions from the crystalline phases (calcite and vaterite, #2). The curve for amorphous silica gel (#3) was obtained after removing contributions from crystalline calcite and vaterite. Peak assignments are given based on references.[41,44]

485

Figure 6. Calcite and vaterite scale factors and goodness of the fit (R_w) for the real space refinement of C-S-H gel exposed to CO_2 as a function of time. The data were obtained by fitting the simulated PDFs of crystalline calcium carbonate polymorphs (calcite and vaterite) to the experimental data sets at high r (40 < r < 65 Å).

Figure 7: PDFs of the decalcifying C-S-H gel/amorphous silica gel as a function of the carbonation time after removal of the crystalline contributions from calcite and vaterite. The initial slope, denoted as $-4\pi\rho_0 r$, provides an indication of the evolution of the atomic number density, ρ_0, during the carbonation reaction.

References

1 P. D. Tennis and H. M. Jennings, *Cem. Concr. Res.*, 2000, **30**, 855–863.

2 L. Black, K. Garbev and I. Gee, *Cem. Concr. Res.*, 2008, **38**, 745–750.

3 I. G. Richardson, *Cem. Concr. Res.*, 2008, **38**, 137–158.

4 L. B. Skinner, S. R. Chae, C. J. Benmore, H. R. Wenk and P. J. M. Monteiro, *Phys. Rev. Lett.*, 2010, **104**, 195502.

5 S. Soyer-Uzun, S. R. Chae, C. J. Benmore, H.-R. Wenk and P. J. M. Monteiro, *J. Am.*

Ceram. Soc., 2012, **95**, 793–798.

6 M. Bauchy, M. J. Abdolhosseini Qomi, F.-J. Ulm and R. J.-M. Pellenq, *J. Chem. Phys.*, 2014, **140**, 214503.

7 W.-S. Chiang, G. Ferraro, E. Fratini, F. Ridi, Y.-Q. Yeh, U.-S. Jeng, S.-H. Chen and P. Baglioni, *J. Mater. Chem. A*, 2014, **2**, 12991–12998.

8 L. Pegado, C. Labbez and S. V. Churakov, *J. Mater. Chem. A*, 2014, **2**, 3477–3483.

9 C. E. White, L. L. Daemen, M. Hartl and K. Page, *Cem. Concr. Res.*, 2015, **67**, 66–73.

10 R. J.-M. Pellenq, A. Kushima, R. Shahsavari, K. J. V. Vliet, M. J. Buehler, S. Yip and F.-J. Ulm, *Proc. Natl. Acad. Sci.*, 2009, **106**, 16102–16107.

11 I. G. Richardson, *Acta Crystallogr. Sect. B Struct. Sci. Cryst. Eng. Mater.*, 2013, **69**, 150–162.

12 K. Garbev, P. Stemmermann, L. Black, C. Breen, J. Yarwood and B. Gasharova, *J. Am. Ceram. Soc.*, 2007, **90**, 900–907.

13 L. Black, C. Breen, J. Yarwood, K. Garbev, P. Stemmermann and B. Gasharova, *J. Am. Ceram. Soc.*, 2007, **90**, 908–917.

14 M. Castellote, C. Andrade, X. Turrillas, J. Campo and G. J. Cuello, *Cem. Concr. Res.*, 2008, **38**, 1365–1373.

15 J. Chen, *Cem. Concr. Res.*, 2004, **34**, 1499–1519.

16 P. J. Chupas, K. W. Chapman, C. Kurtz, J. C. Hanson, P. L. Lee and C. P. Grey, *J. Appl. Crystallogr.*, 2008, **41**, 822–824.

17 P. J. Chupas, X. Qiu, J. C. Hanson, P. L. Lee, C. P. Grey and S. J. L. Billinge, *J. Appl. Crystallogr.*, 2003, **36**, 1342–1347.

18 A. Hammersley, *Eur. Synchrotron Radiat. Facil. Intern. Rep. ESRF97HA02T*, 1997.

19 A. P. Hammersley, S. O. Svensson and A. Thompson, *Nucl. Instrum. Methods Phys. Res. Sect. Accel. Spectrometers Detect. Assoc. Equip.*, 1994, **346**, 312–321.

20 H. M. Rietveld, *J. Appl. Crystallogr.*, 1969, **2**, 65–71.

21 L. Lutterotti, M. Bortolotti, G. Ischia, I. Lonardelli and H.-R. Wenk, *Z. Krist. Suppl.*, 2007, **2007**, 125–130.

22 F. Battocchio, P. J. M. Monteiro and H.-R. Wenk, *Cem. Concr. Res.*, 2012, **42**, 1534–1548.

23 H. Chessin, W. C. Hamilton and B. Post, *Acta Crystallogr.*, 1965, **18**, 689–693.

24 J. Wang, F. Zhang, J. Zhang, R. C. Ewing, U. Becker and Z. Cai, *J. Cryst. Growth*, 2014, **407**, 78–86.

25 J. Wang and U. Becker, *Am. Mineral.*, 2009, **94**, 380–386.

26 T. Egami and S. J. L. Billinge, *Underneath the Bragg Peaks: Structural Analysis of Complex Materials*, Pergamon, Elmsford NY, 2003.

27 X. Qiu, J. W. Thompson and S. J. L. Billinge, *J. Appl. Crystallogr.*, 2004, **37**, 678–678.

28 C. L. Farrow, P. Juhas, J. W. Liu, D. Bryndin, E. S. Bozin, J. Bloch, T. Proffen and S. J. L. Billinge, *J. Phys. Condens. Matter*, 2007, **19**, 335219.

29 C. E. White, J. L. Provis, B. Bloomer, N. J. Henson and K. Page, *Phys Chem Chem Phys*, 2013, **15**, 8573–8582.

30 E. Mugnaioli, I. Andrusenko, T. Schüler, N. Loges, R. E. Dinnebier, M. Panthöfer, W. Tremel and U. Kolb, *Angew. Chem. Int. Ed.*, 2012, **51**, 7041–7045.

31 L. N. Plummer and E. Busenberg, *Geochim. Cosmochim. Acta*, 1982, **46**, 1011–1040.

32 E. Dubina, L. Korat, L. Black, J. Strupi-Šuput and J. Plank, *Spectrochim. Acta. A. Mol. Biomol. Spectrosc.*, 2013, **111**, 299–303.

33 A. Morandeau, M. Thiéry and P. Dangla, *Cem. Concr. Res.*, 2014, **56**, 153–170.

34 E. Drouet, PhD Thesis, ENS Cachan, 2010.

35 Z. Sauman, *Cem. Concr. Res.*, 1971, **1**, 645–662.

36 N. Hyvert, A. Sellier, F. Duprat, P. Rougeau and P. Francisco, *Cem. Concr. Res.*, 2010, **40**, 1582–1589.

37 J. D. Rodriguez-Blanco, S. Shaw and L. G. Benning, *Nanoscale*, 2011, **3**, 265–271.

38 A. Morandeau, M. Thiéry and P. Dangla, *Cem. Concr. Res.*, 2015, **67**, 226–236.

39 V. Morales-Florez, N. Findling and F. Brunet, *J. Mater. Sci.*, 2012, **47**, 764–771.

40 K. Kamiya, A. Oka, H. Nasu and T. Hashimoto, *J. Sol-Gel Sci. Technol.*, 2000, **19**, 495–499.

41 C. Meral, C. J. Benmore and P. J. M. Monteiro, *Cem. Concr. Res.*, 2011, **41**, 696–710.

42 A. F. Wallace, L. O. Hedges, A. Fernandez-Martinez, P. Raiteri, J. D. Gale, G. A. Waychunas, S. Whitelam, J. F. Banfield and J. J. D. Yoreo, *Science*, 2013, **341**, 885–889.

43 J. W. Singer, A. Ö. Yazaydin, R. J. Kirkpatrick and G. M. Bowers, *Chem. Mater.*, 2012, **24**, 1828–1836.

44 F. M. Michel, J. MacDonald, J. Feng, B. L. Phillips, L. Ehm, C. Tarabrella, J. B. Parise and R. J. Reeder, *Chem. Mater.*, 2008, **20**, 4720–4728.